Supermode dispersion and waveguide-to-slot mode transition in arrays of silicon-on-insulator waveguides

Charles E. de Nobriga,[1,*] Gareth D. Hobbs,[1] William J. Wadsworth,[1] Jonathan C. Knight,[1] Dmitry V. Skryabin,[1] Antonio Samarelli,[2] Marc Sorel,[2] and Richard M. De La Rue[2]

[1]*Centre for Photonics and Photonic Materials, Department of Physics, University of Bath, Claverton Down, Bath, BA2 7AY, UK*

[2]*Department of Electronics and Electrical Engineering, University of Glasgow, Rankine Building, Oakfield Avenue, Glasgow, G12 8LT, UK*

**Corresponding author: py3cedn@bath.ac.uk*

Received June 3, 2010; revised October 15, 2010; accepted October 22, 2010; posted October 26, 2010 (Doc. ID 129525); published November 22, 2010

In this Letter, we report group index measurements of the supermodes of an array of two strongly coupled silicon-on-insulator waveguides. We observe coupling-induced dispersion that is greater than the material and waveguide dispersion of the individual waveguides. We demonstrate that the system transforms from supporting the two supermodes associated with two coupled waveguides to the single mode of a slot waveguide within the investigated spectral range. During the cutoff of the antisymmetric supermode, an anti-crossing between the symmetric TM and antisymmetric TE supermodes has been observed. © 2010 Optical Society of America

OCIS codes: 230.7370, 250.5300.

Ultrafast nonlinear photonics in structured materials is a topic of intense current interest [1–3]. Silicon-on-insulator waveguide technology has been demonstrated to have great potential in this area; nanoscale silicon waveguides, or photonic wires, in particular, have offered a promising platform for the realization of nonlinear photonic microchips.

Recent efforts have yielded some understanding of nonlinear propagation effects in single silicon-on-insulator photonic wires [4], but arrays of such photonic wires, both weakly and strongly coupled, have also received great attention [5,6]. The large coupling-induced dispersion in closely spaced waveguide arrays is well understood [7,8]. Given strong enough coupling, the group-velocity dispersion of the supermode with the highest spatial frequency can be shifted from the normal into the anomalous dispersion regime [6]. Solitonic behavior can thus be observed at wavelengths where it is not supported by a single wire.

Parallel to this, it has been shown that high intensities can be achieved in the low-index slot between high-index photonic wires [9], yielding applications across many areas of nonlinear optics, including nonlinear switching [10]. Nonlinear effects in photonic wire arrays can be enhanced by working in the slot mode regime where the magnitude of the electric field vector can be greatly increased. Suitable materials can potentially be inserted into the slot to increase the nonlinear response while reducing the effects of two-photon and free-carrier absorption relative to the coupled ridge regime [8]. The transition between the ridge and slot guidance regimes is studied experimentally in this Letter.

The waveguide arrays studied in this work were fabricated on a silicon-on-insulator (SOI) wafer consisting of a 220-nm-thick silicon guiding layer, insulated from the silicon substrate by a 2-μm-thick layer of silica. Waveguide patterning was achieved through the use of electron beam lithography in hydrogen silsequioxane (HSQ), which was transferred to the guiding layer via fluorine-based inductively coupled plasma reactive ion etching [11]. The chosen combination of etch mask and gas provided good sidewall verticality [Fig. 1(a)] and minimal edge roughness [Fig. 1(b)], ensuring low propagation losses. A slight over-etch, to ensure complete etching of the silicon guiding layer, produced waveguides with a near perfect rectangular cross section on top of a 20-nm-thick silica pedestal [Fig. 1(c)]. The waveguides were thus surrounded by air on two sides, by a residual 160-nm-thick HSQ mask on top and silica underneath.

Coupling-induced supermode dispersion in waveguide arrays has been demonstrated for arrays with larger wall-to-wall spacing [12]. In this work we consider arrays with

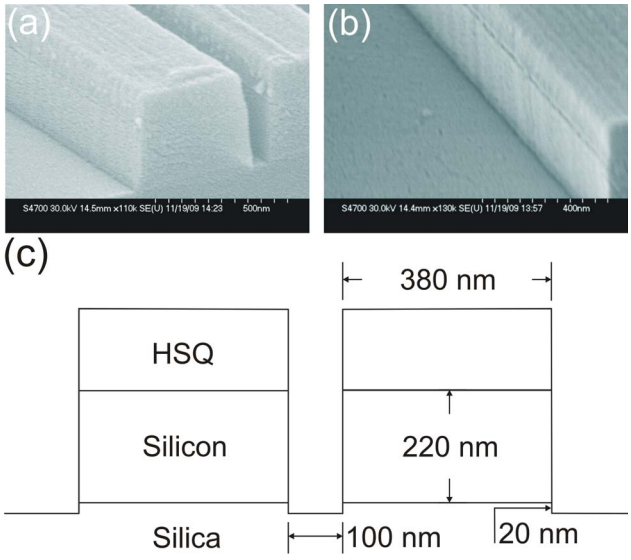

Fig. 1. (Color online) Scanning electron microscope images showing the (a) sidewall verticality and (b) surface roughness of silicon photonic wires produced on the same chip as those used in the following experiments. (c) Schematic of the array used in the experiment. The waveguides are 380 nm × 220 nm in cross section and 3 mm long. The 160-nm-thick residual HSQ layer and the 20 nm silica pedestal created due to the complete etching of the silicon guiding layer are clearly shown.

shorter coupling lengths, ~0.2 mm at 1500 nm, drastically increasing the coupling-induced dispersion and reducing the wavelength of the transition to the slot regime [10]. The geometry studied was a pair of coupled rectangular silicon waveguides with 220 nm height and 380 nm width, with a 100 nm wall-to-wall separation and a total length of 3 mm.

Spectral group index measurements were performed using low-coherence white-light interferometry in a free-space Mach–Zehnder configuration. An optical supercontinuum extending from 400 to 2300 nm produced using a 1064 nm Q-switched microchip laser and a length of solid-core photonic crystal fiber was used as the light source. To prevent thermal and optical damage to the silicon, wavelengths below 1200 nm were removed from the input spectrum by a low-pass (long wavelength) filter. The resultant beam was coupled using bulk objective lenses (60×, NA = 0.65) into and out of the waveguides located in the fixed length arm of the interferometer. Repeatable coupling was ensured through the use of a cw distributed-feedback diode laser at 1510 nm and an InGaAs IR camera. This allowed output field patterns and top-scattered light to be imaged to help optimize input coupling. The reference arm delay was controlled via a planar mirror mounted on a motorized stage, while lenses identical to those in the sample arm were positioned in the reference arm to ensure that only the dispersive effects from propagation in the waveguide array contributed to the measured group delay.

Interferograms were recorded at 17 different wavelengths between 1200 and 2000 nm using 10 nm bandpass filters, with the fringes due to the two

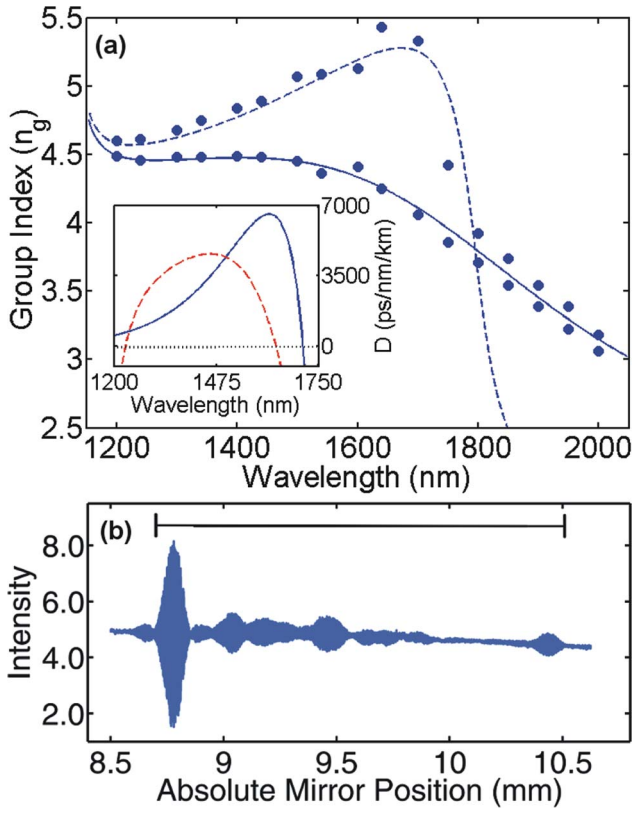

Fig. 2. (Color online) (a) Group index of the symmetric and antisymmetric TE supermodes in a two-channel array. Experimental measurements of the quickest and slowest edges of the observed interferograms are shown by filled circles. The numerically modeled group index is also shown for the symmetric (solid curve) and antisymmetric (dashed curve) TE supermodes. The inset shows the computed dispersion of the TE supermode for a single 380 nm channel (dashed curve) compared to the coupling-induced dispersion (solid curve). (b) Example measured interferogram for the TE supermode at 1700 nm. The horizontal bar denotes the physical extent as described in the text.

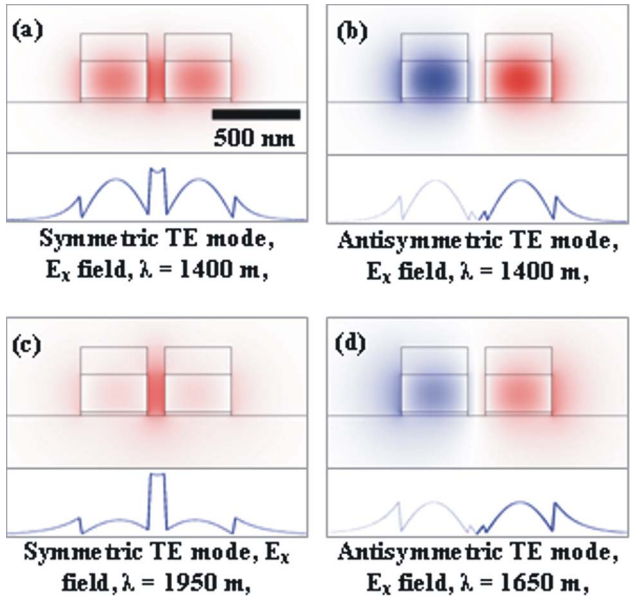

Fig. 3. (Color online) Modeled field plots of the transverse electric field are shown for (a) the symmetric TE supermode and (b) the antisymmetric TE supermode at 1400 nm, long before the ridge–slot transition. For the antisymmetric mode, the left-hand lobe of the field plot and line plot is negative. The antisymmetric supermode is also shown in (d) as it approaches cutoff, at a wavelength of 1650 nm. After cutoff, only the symmetric TE supermode exists. This is shown at 1950 nm in (c). Below each plot is a line plot horizontally through the center of the waveguides.

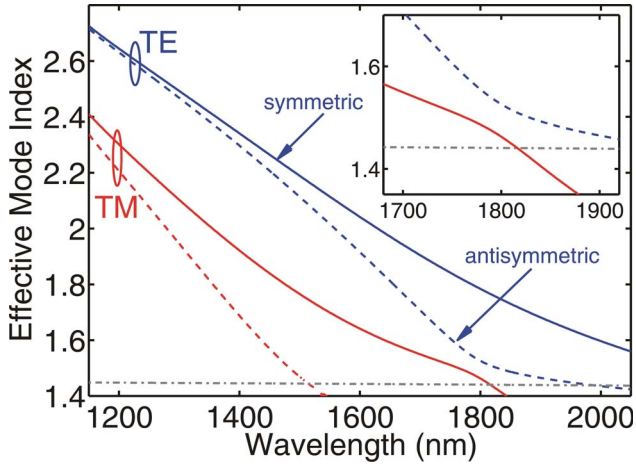

Fig. 4. (Color online) Graph showing the modeled effective indices of the symmetric (solid curve) and antisymmetric (dashed curve) TE and TM supermodes of the two channel array, along with the refractive index of silica (dashed–dotted curve). An anticrossing between the symmetric TM and antisymmetric TE supermodes has been expanded (inset).

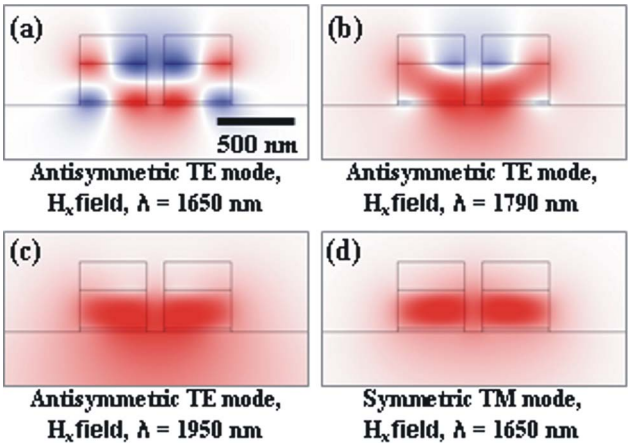

Fig. 5. (Color online) Field plots of the transverse magnetic component (parallel to the silica substrate) of the antisymmetric TE supermode as it passes through the anti-crossing [(a) at 1650 nm, (b) 1790 nm, and (c) 1950 nm]. For comparison, the same component of the symmetric TM mode is shown in (d) at 1650 nm.

polarization states isolated using a polarizer. The resulting interferograms [Fig. 2(b)] showed two distinct peaks separated by a long modulated interference fringe. For each bandpass filter, the mirror positions at the points at which the fringe intensity rose from and dropped to the background level were recorded. By comparison to the modeled data [Fig. 2(a)] it can be concluded that the extremal peaks of the interferogram are associated with propagation over the entire length of the array in the symmetric mode, when the reference arm is shorter, or the antisymmetric mode, when the reference arm is longer. The results clearly show a widening of the interferogram associated with the coupling-induced dispersion [Fig. 2(a)] and then a sharp shrinking at 1700 nm. Beyond 1800 nm, the interferograms are limited by the input spectral width, and are exactly the same as the reference fringes, taken when the sample was not present. Thus 1800 nm marks the transition to a single mode interferogram.

To model the system, an eigenvalue solver (Comsol Multiphysics) was used to solve Maxwell's equations in an idealized geometry, yielding the propagation constants for both the TE (where the dominant electric field component is parallel to the substrate) and the TM supermodes. The TE supermodes are of more interest here as only this polarization supports slot modes. At short wavelengths, two TE supermodes are supported by the array [Figs. 3(a) and 3(b)]. The electric field for the antisymmetric mode is pinned at zero at the center of the slot, due to the supermodal symmetry, and, as such, the expansion of this mode differs greatly from the symmetric case. The dispersion of this mode drastically increases (Fig. 2 inset) so that the decrease in effective index is large. The effective index drops below the refractive index of silica at 1790 nm and the mode is cut off. It can be seen that, for the symmetric mode, high electric fields can exist in the slot over this whole spectral range [Figs. 3(b) and 3(c)]. At longer wavelengths, the system acts as a single slot waveguide, and we would expect the antisymmetric mode to be cut off.

By studying the effective index (Fig. 4) we can see that this is indeed the case, as the effective index of the antisymmetric TE supermode drops below the refractive index of silica. Once this happens, the coupled photonic wire array supports only one mode.

As we approach the cutoff wavelength of the antisymmetric TE mode, the physical geometry adds a complication. Our modeling shows that the asymmetry of the device in the vertical direction, due to the presence of the substrate, leads to vertically asymmetric mode confinement for the antisymmetric TE mode as the wavelength is increased [Figs. 5(a)–5(c)]. This asymmetry yields evolution of the antisymmetric TE mode to the symmetric TM mode and vice versa via an anticrossing. Intuitively this is forbidden by symmetry; however, both these modes have symmetric magnetic fields parallel to the silica substrate.

We have demonstrated the transition between coupled photonic wire and single slot regimes in SOI waveguide arrays and compared the numerical model with experimental results. The results show large coupling-induced dispersion and the cutoff of all but the symmetric TE mode. During this process, we predict an anti-crossing between the symmetric TM and antisymmetric TE supermodes.

The authors thank A. V. Gorbach and W. Ding for many stimulating discussions. This work was funded by the Engineering and Physical Sciences Research Council (EPSRC), grant EP/G044163/1.

References

1. R. M. Osgood, N. C. Paniou, J. I. Dadap, X. Liu, X. Chen, I. W. Hsieh, E. Dulkeith, W. M. Green, and Y. A. Vlasov, Adv. Opt. Photon. **1**, 162 (2009).
2. Q. Lin, O. J. Painter, and G. P. Agrawal, Opt. Express **15**, 16604 (2007).
3. M. A. Foster, A. C. Turner, M. Lipson, and A. L. Gaeta, Opt. Express **16**, 1300 (2008).
4. W. Ding, C. Benton, A. V. Gorbach, W. J. Wadsworth, J. C. Knight, D. V. Skryabin, M. Gnan, M. Sorel, R. M. De La Rue, Opt. Express **16**, 3310 (2008).
5. C. J. Benton, A. V. Gorbach, and D. V. Skryabin, Phys. Rev. A **78**, 033818 (2008).
6. C. J. Benton and D. V. Skryabin, Opt. Express **17**, 5879 (2009).
7. E. Marom, O. G. Ramer, and S. Ruschin, IEEE J. Quantum Electron. **20**, 1311 (1984).
8. M. Wrage, P. Glas, M. Leitner, T. Sandrock, N. N. Elkin, A. P. Nanpartovice, and A. G. Sukharev, Opt. Commun. **175**, 97 (2000).
9. V. R. Almeida, Q. Xu, C. A. Barrios, and M. Lipson, Opt. Lett. **29**, 1209 (2004).
10. C. Koos, P. Vorreau, T. Vallaitis, P. Dumon, W. Bogaerts, R. Baets, B. Esembeson, I. Biaggio, T. Michinobu, F. Diederich, W. Freude, and J. Leuthold, Nat. Photon. **3**, 216 (2009).
11. M. Gnan, S. Thorns, D. S. Macintyre, R. M. De La Rue, and M. Sorel, Electron. Lett. **44**, 115 (2008).
12. C. E. de Nobriga, G. D. Hobbs, W. Ding, A. Gorbach, W. J. Wadsworth, J. C. Knight, D. V. Skryabin, A. Samarelli, M. Sorel, and R. M. De La Rue, in *Conference on Lasers and Electro-Optics/International Quantum Electronics Conference*, OSA Technical Digest (CD) (Optical Society of America, 2010), paper CThB4.